



HAL
open science

A covariate-constraint method to map brain feature space into lower dimensional manifolds

Félix Renard, Christian Heinrich, Marine Bouthillon, Maleka Schenck, Francis Schneider, Stéphane Kremer, Sophie Achard

► To cite this version:

Félix Renard, Christian Heinrich, Marine Bouthillon, Maleka Schenck, Francis Schneider, et al.. A covariate-constraint method to map brain feature space into lower dimensional manifolds. *Network Neuroscience*, 2021, 5 (1), pp.252-273. 10.1162/netn_a_00176 . hal-03165916

HAL Id: hal-03165916

<https://hal.science/hal-03165916>

Submitted on 11 Mar 2021

HAL is a multi-disciplinary open access archive for the deposit and dissemination of scientific research documents, whether they are published or not. The documents may come from teaching and research institutions in France or abroad, or from public or private research centers.

L'archive ouverte pluridisciplinaire **HAL**, est destinée au dépôt et à la diffusion de documents scientifiques de niveau recherche, publiés ou non, émanant des établissements d'enseignement et de recherche français ou étrangers, des laboratoires publics ou privés.

A covariate-constraint method to map brain feature space into lower dimensional manifolds

Félix Renard¹, Christian Heinrich², Marine Bouthillon²,
Maleka Schenck^{3,4}, Francis Schneider^{3,4,5}, Stéphane Kremer^{2,6}, and Sophie Achard¹

¹Univ. Grenoble Alpes, CNRS, Inria, Grenoble INP, LJK, 38000 Grenoble, France

²iCube, Université de Strasbourg, CNRS, 300 boulevard S. Brant, BP 10413, 67412 Illkirch Cedex, France

³Service de Médecine Intensive Réanimation, CHU de Strasbourg, France

⁴Faculté de Médecine FMTS, Strasbourg, France

⁵U1121, Université de Strasbourg, France

⁶Imagerie 2, CHU de Strasbourg, Université de Strasbourg, France

Keywords: Graphs, machine learning, connectomes, hub disruption index

Abstract

Human brain connectome studies aim at both exploring healthy brains, and extracting and analyzing relevant features associated to pathologies of interest. Usually this consists in modeling the brain connectome as a graph and in using graph metrics as features. A fine brain description requires graph metrics computation at the node level. Given the relatively reduced number of patients in standard cohorts, such data analysis problems fall in the high-dimension low sample size framework. In this context, our goal is to provide a machine learning technique that exhibits flexibility, gives the investigator grip on the features and covariates, allows visualization and exploration, and yields insight into the data and the biological phenomena at stake. The retained approach is dimension reduction in a manifold learning methodology, the originality lying in that one (or several) reduced variables be chosen by the investigator. The proposed method is illustrated on two studies, the first one addressing comatose patients, the second one addressing young versus elderly population comparison. The method sheds light

Corresponding author: Félix Renard, felixrenard@gmail.com

24 on the differences between brain connectivity graphs using graph metrics and potential clinical
25 interpretations of these differences.

AUTHOR SUMMARY

26 Human brain connectome studies aim at both exploring healthy brains, and extracting and analyzing
27 relevant features associated to pathologies of interest. Usually this consists in modeling the brain
28 connectome as a graph and in using graph metrics as features. A fine brain description requires graph
29 metrics computation at the node level. Given the relatively reduced number of patients in standard
30 cohorts, such data analysis problems fall in the high-dimension low sample size framework. In this
31 context, our goal is to provide a machine learning technique that exhibits flexibility, gives the investigator
32 grip on the features and covariates, allows visualization and exploration, and yields insight into the data
33 and the biological phenomena at stake. The retained approach is dimension reduction in a manifold
34 learning methodology, the originality lying in that one (or several) reduced variables be chosen by the
35 investigator. The proposed method is illustrated on two studies, the first one addressing comatose
36 patients, the second one addressing young versus elderly population comparison. The method sheds light
37 on the differences between brain connectivity graphs using graph metrics and potential clinical
38 interpretations of these differences.

INTRODUCTION

39 Brain modeling and understanding is a very active field of research involving different disciplines, such
40 as neuroscience, image and signal processing, statistics, physics, and biology. These last years,
41 neuroimaging modalities have been developed to explore the brain for both structural and functional
42 features. It is now recognized that these images are providing very promising noninvasive observations of
43 the brain (Bullmore & Sporns, 2009b; Mwangi, Tian, & Soares, 2014; Richiardi, Achard, Bunke, & Van
44 De Ville, 2013). One consequence of the availability of such massive datasets is the need to develop more
45 and more sophisticated models to unravel the possible alteration of brains due to the impact of different
46 pathologies. In this context, representing the brain as a global system is capital. This may be achieved
47 using a *network* (Bullmore & Sporns, 2009a). A brain network is a graph where nodes correspond to

48 specific regions and edges describe interactions and links between those regions. Different kinds of links
49 and interactions may be of interest. Anatomical tracts are identified using diffusion imaging (Sporns,
50 Tononi, & Kötter, 2005) and used in anatomical connectivity studies, where the whole set of links is
51 called an *anatomical connectome*. Functional interactions are identified in functional imaging studies,
52 whether in resting-state or in task-performing (Fallani, Richiardi, Chavez, & Achard, 2014; Rosazza &
53 Minati, 2011), and used in functional connectivity studies. The whole set of functional links is called a
54 *functional connectome*. In the functional case, brain networks are particularly adequate in encapsulating
55 both spatial and temporal information in a single model. Indeed, brain networks are constructed using
56 brain parcellation, namely spatial features, and time series interactions, namely temporal features. This
57 model has attracted lots of attention these last twenty years by providing both very intuitive and spatial
58 maps of brain networks.

59 Brain networks can be quantified using graph metrics such as minimum path length, clustering (Watts &
60 Strogatz, 1998), global and local efficiency (Latora & Marchiori, 2001), modularity (Newman, 2006),
61 and assortativity (Newman, 2002), among others. As these metrics are associated to specific network
62 features, it is often possible to find the appropriate metrics to use given specific neuroscience hypotheses
63 of the study. For the study of brain disorders, these metrics have been used in order to extract biomarkers
64 for pathologies such as for example Alzheimer's disease (Supekar, Menon, Rubin, Musen, & Greicius,
65 2008), schizophrenia (Lynall et al., 2010), and multiple sclerosis (Filippi et al., 2014). Extracting
66 quantitative parameters of brain networks is compulsory to conduct any statistical analysis. In this
67 framework, statistical and machine learning approaches on graph metrics on all nodes allow the
68 quantification of differences between groups (Richiardi et al., 2013).

69 For any dataset, any graph metric can be computed either at the global level with one value for an entire
70 network or at the nodal level with one value for each node and a vector of values for the entire network. It
71 has already been shown that global values may not discriminate two groups of subjects (Achard et al.,
72 2012), which shows their limits as biomarkers. Few attempts have been made to use directly distances
73 between networks such as the edit distance (Mokhtari & Hossein-Zadeh, 2013), or network similarities
74 (Mheich et al., 2017). However, nodal level approaches are challenging since hundreds of brain areas can
75 be extracted whereas the number of subjects is generally small. This corresponds to the High Dimension
76 Low Sample Size (HDLSS) configuration and falls under the curse of dimensionality (Bellman, 1961). In

77 particular, standard classification and regression algorithms are not robust anymore in such a context
78 (chapter 2 section 5 and chapter 18 of (Hastie, Tibshirani, & Friedman, 2001)).

79 Dimension reduction techniques tackle curse of dimensionality issues (Hastie et al., 2001). In this
80 framework, feature selection, where a subset of the original variables is considered, and feature
81 extraction, where the original variables are transformed to a smaller set, may be envisaged (Webb, 2002).
82 We resort here to the ISOMAP methodology, which is a well-known nonlinear feature extraction
83 algorithm generalizing Principal Component Analysis dimension reduction (Huo, Ni, & Smith, 2007;
84 Tenenbaum, de Silva, & Langford, 2000). ISOMAP may be seen as a manifold learning approach, where
85 the degrees of freedom of the data are captured by the latent variables, and where the structure of points
86 in the latent space (the reduced space) mimics the structure of data in the original space. Nevertheless,
87 ISOMAP raises two issues: interpreting the latent variables and determining the effect a change in the
88 latent variables incurs in the data space, that is the corresponding changes in brain networks and the
89 underlying neuroscience hypotheses at stake in the case of the present study.

90 Dimension reduction is not new in the field of brain connectivity studies. Several methods have been
91 proposed to extract nodal features at the level of brain regions. Using the Hub Disruption Index (the κ
92 index) to analyze a set of brain networks may be considered as a feature extraction approach: this is a
93 user-defined transformation of the original space to a 1D latent space (Achard et al., 2012). Principal
94 Component Analysis (PCA) was previously applied on graph metrics in (Robinson, Hammers, Ericsson,
95 Edwards, & Rueckert, 2010) with vectors representing brains at the nodal level. We proposed in (Renard,
96 Heinrich, Achard, Hirsch, & Kremer, 2012) to use kernel PCA, a nonlinear version of PCA. Besides,
97 interpreting latent variables may be addressed by correlating the reduced space with clinical data (Gerber,
98 Tasdizen, Thomas Fletcher, Joshi, & Whitaker, 2010). Covariates may also be mapped or regressed on the
99 reduced space as proposed in (Aljabar, Wolz, & Rueckert, 2012), thus shedding light on latent variables.
100 Dimension reduction methods have also been applied to connectivity matrices (Ktena et al., 2018; Kumar,
101 Toews, Chauvin, Colliot, & Desrosiers, 2018; Yamin et al., 2019) or to the voxels time series (Saggar et
102 al., 2018) mainly for classification purposes. It is indeed difficult using the whole connectivity matrices
103 or voxels time series to give an interpretation at the nodal or voxel level (Gallos & Siettos, 2017; Haak,
104 Marquand, & Beckmann, 2018; Laurienti et al., 2019). Network embedding framework can be viewed as
105 a dimension reduction method and was also applied to brain connectivity graphs (Rosenthal et al., 2018).

106 The objective of this article is to integrate all features cited above in one method: working at the nodal
107 level, applying dimension reduction techniques, and mapping covariates to ease interpretation. In
108 addition, a new methodology is proposed to incorporate interesting networks features already identified
109 in specific datasets directly in the manifold learning approach. Contrary to statistical tests at nodal levels
110 where each feature is treated independently of others, our approach based on machine learning is able to
111 analyze joint variations between local descriptors.

112 This paper is focusing on two already published datasets. The first one consists in fMRI datasets on 20
113 healthy controls and 17 coma patients from Achard *et al.* (Achard *et al.*, 2012). The second one is based
114 on (Achard & Bullmore, 2007) where 15 young healthy subjects and 11 elderly healthy subjects were
115 scanned using resting state fMRI. Our first experiment compares data driven approaches such as Linear
116 Discriminant Analysis (LDA) and Random Forests (RF) to an ad hoc description such as the hub
117 disruption index κ . This allows to compare classical machine learning approaches where the
118 interpretability of the results is often difficult with approaches resorting to descriptors constructed using
119 neuroscientific hypotheses. This first experiment can be seen as preliminaries of the sequel of the paper,
120 where a feature is extracted for each individual in order to optimize classification of the two groups either
121 using classical machine learning approaches or ad hoc descriptors. The second experiment consists in
122 constructing a data-driven manifold, ISOMAP, using the graph metrics as features. ISOMAP is providing
123 a compact representation of brain connectomes in a reduced space where it is straightforward to map the
124 available covariates. In addition, we may interpret changes in connectomes by regressing covariables like
125 κ on the reduced space using latent variables.

126 This representation allows a visualization of each subject relatively to the whole population, which is
127 crucial in clinical studies for example in order to better understand brain changes for each specific
128 subject. Besides, κ has been shown to be both a meaningful descriptor and a good classifying feature for
129 brain connectomes of coma patients. Therefore, we propose a new method based on a covariate
130 constrained manifold learning (CCML) using κ as an input of ISOMAP. This allows us to propose a new
131 generative model based on our new data representation, to better predict the variation in each patient
132 given the changes of covariables. Based on the results of the first experiment, the choice of the covariate,
133 κ in this work, can be adjusted to the studied data sets.

MATERIALS AND METHODS

134 *Resting state fMRI data*

135 *Comatose study* The data were acquired in a previous study aimed at characterizing resting state
136 connectivity brain networks for patients with consciousness disorders. The description of the data and
137 results is reported in (Achard et al., 2012). The patients were scanned a few days after major acute brain
138 injury, when sedative drug withdrawal allowed for spontaneous ventilation. Therefore, all patients were
139 spontaneously ventilating and could be safely scanned at the time of fMRI. The causes of coma are
140 patient-dependent: 12 had cardiac and respiratory arrest due to various causes; 2 had a gaseous
141 cerebrovascular embolism; 2 had hypoglycemia; and 1 had extracranial artery dissection. A total of
142 twenty-five patients were scanned (age range, 21-82 y; 9 men). Data on eight patients were subsequently
143 excluded because of unacceptable degrees of head movement. The coma severity for each patient was
144 clinically assessed using the 62 items of the WHIM scale: scores range from 0, meaning deep coma, to
145 62, meaning full recovery. Six months after the onset of coma, 3 patients had totally recovered, 9 patients
146 had died, and 5 patients remained in a persistent vegetative state. The normal control group is composed
147 of 20 healthy volunteers matched for sex (11 men) and approximately for age (range, 25-51 y) to the
148 group of patients. This study was approved by the local Research Ethics Committee of the Faculty of
149 Health Sciences of Strasbourg on October 24, 2008 (CPP 08/53) and by the relevant healthcare
150 authorities. Written informed consent was obtained directly from the healthy volunteers and from the
151 next of kin for each of the patients. Resting-state data were acquired for each subject using gradient echo
152 planar imaging technique with a 1.5-T MR scanner (Avanto; Siemens, Erlangen, Germany) with the
153 following parameters: relaxation time = 3 s, echo time = 50 ms, isotropic voxel size = $4 \times 4 \times 4 \text{ mm}^3$,
154 405 images, and 32 axial slices covering the entire cortex. The preprocessing of the data is detailed in our
155 previous study (Achard et al., 2012).

156 *Young and elderly study* The data used in this study have already been analyzed in two papers (Achard
157 & Bullmore, 2007) and (Meunier, Achard, Morcom, & Bullmore, 2009). The goal of these papers was to
158 identify the changes in brain connectomes for elderly subjects in terms of topological organization of
159 brain graphs. The data consist of 15 young subjects aged 18-33 years, mean age=24 and 11 elderly
160 subjects aged 62-76 years. Each subject was scanned using resting-state fMRI as described in (Achard &

161 [Bullmore, 2007](#)) (Wolfson Brain Imaging Centre, Cambridge, UK). For each dataset, a total of 512
162 volumes was available with number of slices, 21 (interleaved); slice thickness, 4 mm; interslice gap, 1
163 mm; matrix size, 64×64 ; flip angle, 90° ; repetition time (TR), 1100 ms; echo time, 27.5 ms; in-plane
164 resolution, 3.125 mm.

165 *Preprocessing and wavelet graph estimation*

166 Brain network graphs were determined following ([Achard et al., 2012](#)) for comatose study and ([Achard](#)
167 [& Bullmore, 2007](#)) for young and elderly study. For each subject, data were corrected for head motion
168 and then coregistered with each subject's T1-weighted structural MRI. Each subject's structural MRI was
169 nonlinearly registered with the Colin27 template image. The obtained deformation field image was used
170 to map the fMRI datasets to the automated anatomical labeling (AAL) or to a customized parcellation
171 image with 417 anatomically homogeneous size regions based on the AAL template image
172 ([Tzourio-Mazoyer et al., 2002](#)). Regional mean time series were estimated by averaging the fMRI time
173 series over all voxels in each parcel, weighted by the proportion of gray matter in each voxel of the
174 segmented structural MRIs. We estimated the correlations between wavelet coefficients of all possible
175 pairs of the $N = 90$ or 417 cortical and subcortical fMRI time series extracted from each individual
176 dataset. For the coma, only scale 3, 0.02-0.04 Hz, wavelet correlation matrices were considered. For the
177 young and elderly, the wavelet scale considered corresponds to 0.06-0.11 Hz. The choice of these
178 wavelet scales or frequency bands is explained precisely in the corresponding papers ([Achard &](#)
179 [Bullmore, 2007](#); [Achard et al., 2012](#)). To generate binary undirected graphs, a minimum spanning tree
180 algorithm was applied to connect all parcels. The absolute wavelet correlation matrices were thresholded
181 to retain 2.5 % of all possible connections. Each subject was then represented by a graph with nodes
182 corresponding to the same brain regions, and with the same number of edges.

183 *Graph metrics*

184 The objective is to extract differences between the two groups with respect to the topological
185 organization of the graphs. Each graph is summarized by graph metrics computed at the nodal level.
186 Three metrics are considered here: degree, global efficiency, and clustering ([Bullmore & Sporns, 2009b](#)).

The degree is quantifying the number of edges belonging to one node. Let G denote a graph with $G_{ij} = 0$ when there is no edge between nodes i and j , and $G_{ij} = 1$ when there is an edge between nodes i and j .

The degree D_i of node i is computed as

$$D_i = \sum_{j \in G, j \neq i} G_{ij}. \quad (1)$$

The global efficiency measures how the information is propagating in the whole network. A random graph will have a global efficiency close to 1 for each node, and a regular graph will have a global efficiency close to 0 for each node. The global efficiency E_{glob} is defined as the inverse of the harmonic mean of the set of the minimum path lengths L_{ij} between node i and all other nodes j in the graph:

$$E_{glob_i} = \frac{1}{N-1} \sum_{j \in G} \frac{1}{L_{ij}} \quad (2)$$

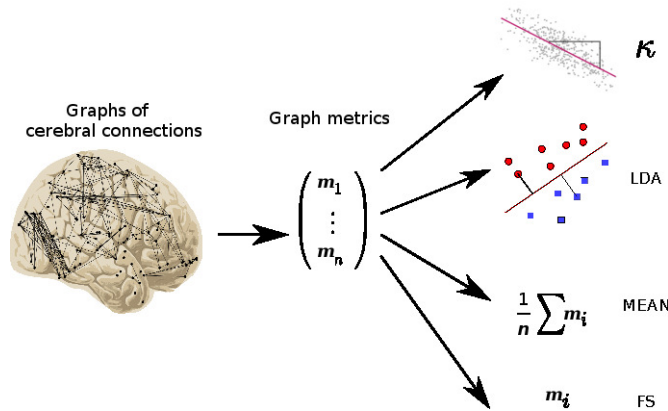
Clustering is a local efficiency measure corresponding to information transfer in the immediate neighborhood of each node, defined as:

$$Clust_i = \frac{1}{N_{G_i}(N_{G_i} - 1)} \sum_{j, k \in G_i, j \neq k} \frac{1}{L_{jk}}, \quad (3)$$

187 where G_i is the subgraph of G defined by the set of nodes that are the nearest neighbors of node i . A high
 188 value of clustering corresponds to highly connected neighbors of each node, whereas a low value means
 189 that the neighbors of each node are rather disconnected.

190 Each graph metric emphasizes a specific property at the nodal level. With a view to statistical
 191 comparison, several methods have already been developed, representing data in specific spaces. Each
 192 method aims at separating classes. Usually these methods are very general and can be applied without
 193 careful inspection of the data. We used here four different methods ([Richiardi, Achard, Bullmore, &](#)
 194 [Ville, 2011](#)): the κ index resulting from a careful inspection of the data, mean over graph metrics
 195 (denoted here MEAN), LDA and Feature Selection (FS) by selecting the best feature based on a
 196 univariate statistical Student t-test. Like the κ index, each of these methods provides, for each patient, a
 197 scalar feature corresponding to particular property of the data. Figure 1 gives an illustration of the
 198 different methods.

203 ***κ index definition***



199 **Figure 1.** General framework from graphs of cerebral connectomes to the different scalar features. Brain connectivity graphs are extracted from fMRI data.
 200 Graph metrics are computed at the nodal level for each subjects. The matrices of graph metrics can then be analysed using different methods: the hub disruption
 201 index based on regression analyses (κ); Linear Discriminant Analysis (LDA); average of metrics (MEAN); and Feature Selection (FS). Each of these methods
 202 allow to summarize the graph metric in one scalar for each subject in order to better differentiate the studied populations.

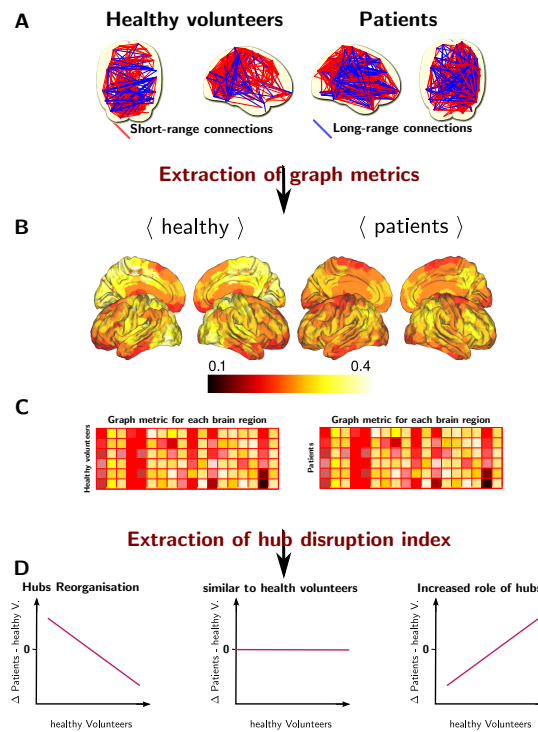
In our previous study (Achard et al., 2012), κ was devised to compare graph metrics obtained on each node of a subject or of a group with reference group (see figure 2). In classical comparisons between a group of patients and a group of healthy volunteers, the reference is the group of healthy volunteers. In the present study, for a given graph metric and two groups, we first compute the average of this metric for each node over the group of healthy volunteers, denoted as the reference. Each subject is then summarized as a vector of values of dimension the number of nodes. Then, for each patient, κ corresponds to the slope of the regression of a nodal graph metric between the given patient minus the reference and the reference. Let N denote the number of nodes in the graph, n_p the number of patients, and n_c the number of controls. Let $(m_1, \dots, m_{n_p}) \in \mathbb{R}^{N \times n_p}$ denote a matrix of graph metric extracted given the graphs of patients, for j , $1 \leq i \leq n_p$, $m_j \in \mathbb{R}^N$. For each j , m_j is equal to one graph metric such as D , $Eglob$ or $Clust$. Let us also define a similar matrix for the controls, $(h_1, \dots, h_{n_c}) \in \mathbb{R}^{N \times n_c}$. Let us define the average metric for controls, for each i , $1 \leq i \leq N$,

$$\bar{h}_i = \frac{1}{n_c} \sum_{j=1}^{n_c} h_{ij} \quad (4)$$

κ is defined by the following regression:

$$m_i - h_i = \kappa \bar{h}_i + \epsilon_i, \quad (5)$$

208 where ϵ_i is the classical error term in linear regression. In order to give a simple interpretation of κ , we
 209 assume that the global graph metric computed as an average over the nodes is the same in both groups. A
 210 value of zero for κ is showing that the graph metric obtained at the node level is the same for the patient
 211 and the reference. A positive value of κ is indicating that the hubs and non-hubs of the patient in
 212 comparison to the reference are located on the same nodes. However, the values of the graph metrics are
 213 increased for the hubs and decreased for the non-hubs. Finally, when the value of κ is negative, the hubs
 214 of the reference are no longer hubs of the patient, and the non-hubs of the reference are hubs for the
 215 patient. In (Achard et al., 2012), we showed that the κ index is able to discriminate both groups (coma
 216 patients and healthy volunteers) while the global metric is unable to identify any significant difference.
 217 Instead of averaging the graph metrics, the κ index is capturing a joint variation of the metrics computed
 for each node.



204 **Figure 2.** Extraction of hub disruption index κ : A. brain connectomes inferred for each subjects; B. for each brain connectome, extraction of graph metrics
 205 for each region of the brain; C. matrix representation of the graph metrics where a row corresponds to a subject and a column corresponds to a brain region; D.
 206 computation of the hub disruption index by regressing the average of brain metrics of the difference of patients and average of healthy volunteers against the
 207 average of healthy volunteers. The hub disruption index corresponds to the slope coefficient. We give several illustrations following the sign of this coefficient.

218

219 ***Mean over the nodes (MEAN)***

220 For each graph metric, the mean over the nodes of the graph captures a global property of the network.
221 These global metrics have been previously used to discriminate two populations of networks, for example
222 for Alzheimer’s disease (Supekar et al., 2008) and for schizophrenia (Lynall et al., 2010). Such a
223 coefficient can discriminate well two networks when their topologies are really different. However, such
224 metrics do not take into account the specificity of the nodes. Indeed, when permuting the nodes of the
225 graph, the global metric is not changed, but the hubs of the graph are not associated to the same nodes
226 anymore. Therefore, a graph reorganization cannot be detected using such global metrics.

227 ***Linear discriminant analysis (LDA)***

228 LDA (Fisher, 1936) is a classification method, aiming at identifying the linear projection optimally
229 separating two groups. It can be considered as a gold standard for linear group discrimination. It is not
230 specific to the analysis of networks.

231 LDA has been previously used for network discrimination in (Robinson et al., 2010). This algorithm
232 amounts to computing a scalar for each graph. However, there is no simple clinical interpretation of the
233 discriminating parameter.

234 ***Feature Selection (FS)***

235 As for LDA, FS determines the features yielding the best separation of the two groups. Several features
236 may be used simultaneously. In order to establish a fair comparison with the other methods, we choose to
237 extract the single feature yielding the best separation. Several methods exist for FS. We choose univariate
238 FS implemented in (Pedregosa et al., 2011). An advantage of FS is that it is capturing discriminative
239 features at the node level. As the selected features are extracted directly from the data, it is usually
240 possible to derive a clinical interpretation. However, joint variations are not modeled and on the comatose
241 study, FS is not able to yield results of the same quality as those obtained using κ .

242 ***Modeling populations of networks with manifold learning***

243 ISOMAP (Tenenbaum et al., 2000) is used as a manifold learning approach to describe population
244 networks. We propose here an original approach based on ISOMAP, where we constrain one variable of
245 the reduced space (the latent space) to correspond to a covariate.

246 *Manifold learning using ISOMAP* ISOMAP devises a reduced dimension version of the original set of
247 points. Interpoint distances in the reduced space reproduce as much as possible interpoint distances in the
248 original space. Euclidean and geodesic distances are respectively used. Principal component analysis
249 may be seen as a particular case of ISOMAP, where Euclidean distances are used in the original space,
250 instead of geodesic distances. The reader is referred to (Tenenbaum et al., 2000) for details about the
251 algorithm.

252 In our case, the original data correspond to a vector of graph metrics for each subject, the dimension of
253 the vector being the number of nodes times the number of metrics. For each analysis, only one metric is
254 considered here. However, this method could be applied using jointly several metrics. Covariates may be
255 regressed on the reduced space. In the present work, this was achieved using a classic radial basis
256 function interpolation.

257 The choice of the ISOMAP is two fold: firstly, the estimated reduced space is a smooth manifold, and
258 preserves the global structure of the dataset. Notably, the reduced space exhibits a continuum function of
259 subjects. Secondly, the cost function of the ISOMAP allows the integration of additional constrained
260 scores. ISOMAP was performed by computing a nearest neighbor graph connecting the four nearest
261 neighbors according to the euclidean distance. This distance reflects correctly the local topology of the
262 graph metrics space. The choice of four neighbors is driven by the relatively small number of subjects in
263 the study.

264 The classification score of the ISOMAP was computed using a non linear Support Vector Machine
265 (SVM) approach with radial basis function kernel in the reduced space Hearst, Dumais, Osuna, Platt, and
266 Scholkopf (1998).

267 *Covariate constrained manifold learning* One drawback of manifold learning algorithms is the difficulty
268 to interpret the reduced coordinates because they are usually meaningless. The original method proposed

269 in this work consists in constraining one coordinate of the reduced space to correspond to a specific
 270 covariate. The other coordinates are left unconstrained, as in classical ISOMAP. Such a procedure
 271 requires special care regarding the optimization aspect. We apply a strategy proposed in [Brucher,](#)
 272 [Heinrich, Heitz, and Armspach \(2008\)](#), where points are introduced one by one.

273 Moreover, a scale factor α is considered for the axis corresponding to the covariate. This parameter,
 274 obtained by optimization, balances the scales of the different axes.

The reduced point $\tilde{\mathbf{x}}_i$ is defined by $\tilde{\mathbf{x}}_i = [\alpha c_i; \mathbf{x}_i]^T$, where c_i is the chosen covariate and \mathbf{x}_i are the other coordinates. The cost function E is defined as:

$$E = \sum_{i,i < j} (\|\tilde{\mathbf{x}}_i - \tilde{\mathbf{x}}_j\|^2 - \|\mathbf{y}_i - \mathbf{y}_j\|^2)^2, \tag{6}$$

275 where $\{\mathbf{y}_i\}_{i=1..N}$ is the graph metric vectors over N graph nodes. For an incoming data point i , the cost
 276 function E is optimized three times with regard to 1) \mathbf{x}_i as $\min_{\mathbf{x}_i} E$, 2) α as $\min_{\alpha} E$ and 3) \mathbf{x}_j for each point
 277 that has already been included as $\min_{\{\mathbf{x}_j\}_{j=1..i-1}} E$. We consider $i < j$ in the sum of the cost function to avoid
 278 counting twice the errors between two samples.

279 The distance in the cost function is the Euclidean one. Since the samples are added sample by sample,
 280 this distance reflects only the local neighborhood of the new added one.

281 To facilitate optimization and to avoid possible local minima, instead of inserting the samples at random,
 282 we choose the sample to be incorporated next as the one with the largest geodesic distance to the samples
 283 already incorporated. Indeed, interpolation problems are always easier than extrapolation problems
 284 where greater uncertainty may occur. We initialize the procedure by taking the two samples with the
 285 largest geodesic distance. The first two samples are used as landmarks of the border of the reduced space,
 286 and the insertion of new samples will generate only small displacements of the already inserted samples.

287 The algorithm is described in Algorithm 1 and available here

288 <https://github.com/renardfe/CCML>.

289 *Application: a generative model for the prediction of the variation in a subject with regard to the changes of a*
 290 *covariate*

Algorithm 1 – covariate constrained manifold learning (CCML)

Input – dataset: N vectors (samples) $\{\mathbf{y}_i\}_{i=1..N}$ of a graph metric over n graph nodes

Result: reduced space representation $\{\tilde{\mathbf{x}}_i\}_{i=1..N}$ of the dataset, where the first coordinate of each $\tilde{\mathbf{x}}_i$ corresponds to the covariate.

Initialization: select the two most distant samples

Determine their reduced coordinates by minimizing E with $\alpha = 1$

Update the scale α by minimizing E wrt α , \mathbf{x}_i fixed, as $\min_{\alpha} E$.

while All points are not included **do**

1) **Select the most distant sample** \mathbf{y}_k to the already selected samples

2) **Compute** \mathbf{x}_k by minimizing E wrt \mathbf{x}_k (α and other \mathbf{x}_i 's fixed) as $\min_{\mathbf{x}_k} E$.

3) **Update the scale** α by minimizing E wrt α (\mathbf{x}_i 's fixed) as $\min_{\alpha} E$.

4) **Update \mathbf{x}_j 's of samples already included** by minimizing E as $\min_{\{\mathbf{x}_j\}_{j=1..k-1}} E$.

end while

From the obtained embedding, a generative model

$$\hat{\mathbf{y}} = f(\tilde{\mathbf{x}}) \tag{7}$$

can be devised, where $\hat{\mathbf{y}}$ is a vector in the original space (the connectome space), $\tilde{\mathbf{x}}$ is a vector from the manifold embedding, and f is a regression function. Multivariate adaptive regression splines (MARS) (Friedman, 1991) is chosen for the regression function f for its nice properties (one regression for each coordinate of f , i.e. n regressions): locally linear and globally nonlinear. The parameters of f can be determined using the dataset $\{\mathbf{y}_i\}_{i=1..N}$ and the corresponding reduced vectors $\{\tilde{\mathbf{x}}_i\}_{i=1..N}$ using equation:

$$\mathbf{y}_i = f(\tilde{\mathbf{x}}_i) + \epsilon_i = \hat{\mathbf{y}}_i + \epsilon_i, \tag{8}$$

291 where ϵ_i is the residual between a sample and its prediction $\hat{\mathbf{y}}_i$. The residuals allow to evaluate the
 292 accuracy of the regression function.

293 This kind of model is not original, PCA being the most well known case where the model is defined as
 294 $\mathbf{y} = \mathbf{A} \tilde{\mathbf{x}} + \epsilon$, see e.g. (Lawrence, 2004; Sfikas & Nikou, 2016) for references. Such a generative model

295 used in the CCML framework allows to determine changes in the original space (the connectome space)
296 generated by a displacement in the reduced space, for example along the covariate axis.

RESULTS

297 The different algorithms have been implemented in the Python language using the scikit learn toolbox
298 (Pedregosa et al., 2011). When left unspecified, coma data are used. The use of the young and elderly
299 data is explicitly stated.

300 *Local analysis using dimension reduction*

301 Permutation tests are performed on the κ index and on the three other measures (LDA, FS, MEAN) to
302 assess the ability of those four metrics to discriminate two populations. More precisely, for each
303 coefficient separately, the difference of the means of the two populations is determined for the observed
304 populations. The labels of the samples are then shuffled and the difference of the means of the shuffled
305 two populations is determined. This latter step is performed 10^4 times. It avoids to make any assumption
306 on the distribution of the statistic. Simultaneously the correlations between the observed κ index and the
307 other coefficients are estimated.

310 The results corresponding to the different methods aiming at discriminating the two groups (control and
311 coma) are given in Table 1. As expected, the machine learning algorithms (ie, *LDA* and *FS*) show good
312 performances in separating the two groups for different graph metrics. This is consistent with the fact that
313 these methods have been tailored to classify the two groups. The results with the κ index show similar
314 performances in separating the two groups. The large correlations between machine learning algorithms
315 on the one hand and the graph metric κ on the other hand show retrospectively that similar performances
316 were to be expected.

317 Besides, a strong relationship can be observed between κ and LDA (correlation scores greater than 0.87
318 for each metric). The FS correlation scores are lower than the LDA correlation ones. The difference
319 between the two methods is that LDA considers a linear combination of features, with a global
320 perspective, whereas FS selects one feature and acts locally. Since κ reflects a global reorganization of
321 the brain, it is expected that the correlation score of LDA be greater than the FS one. Finally, MEAN
322 scores reveal that this measure is not appropriate in this study.

308 **Table 1.** P-value of permutation tests comparing the mean of the two groups (10^4 permutations, which bounds the p-values). The correlation scores are
 309 estimated between the κ index and the three other measures (*LDA*, *FS*, and *MEAN*).

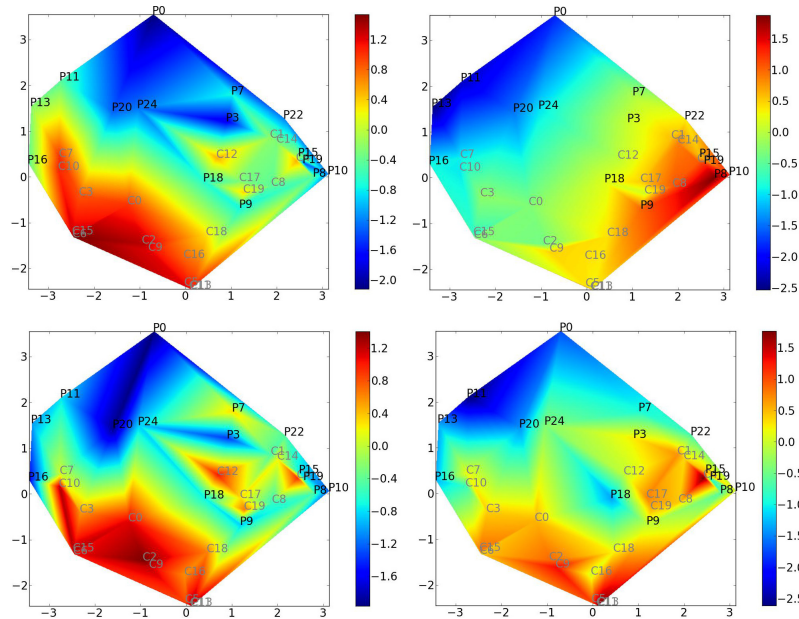
Mean diff. or correlation	<i>Eglob</i> (p-value)	corr. (p-value)	<i>Clust</i> (p-value)	corr. (p-value)	<i>D</i> (p-value)	corr. (p-value)
κ	0.79 ($< 10^{-4}$)		0.75 ($< 10^{-4}$)		0.81 ($< 10^{-4}$)	
<i>LDA</i>	-2.89 ($< 10^{-4}$)	0.88 ($< 10^{-4}$)	-1.78 ($< 10^{-4}$)	0.87 ($< 10^{-4}$)	-2.39 ($< 10^{-4}$)	0.88 ($< 10^{-4}$)
<i>FS</i>	0.12 ($< 10^{-4}$)	0.6 (10^{-4})	-0.5 ($< 10^{-4}$)	-0.66 (10^{-4})	21.93 ($< 10^{-4}$)	0.6 (10^{-4})
<i>MEAN</i>	0.14 (0.58)	0.25 (0.78)	-0.013 (0.43)	-0.19 (0.85)		

323 **Standard ISOMAP manifold learning and the κ index**

327 In this section, the goal is to link the reduced space obtained by manifold learning to different covariates
 328 such as the κ index. We want to assess whether a given covariate varies smoothly across the reduced
 329 space, and is therefore predictable using this space.

330 Figure 3 represents the reduced space obtained using standard ISOMAP, as opposed to using CCML. The
 331 values of the different covariates are color-coded. The reduced space representation allows to separate
 332 both populations. Besides, by visual inspection of the color-coded maps, it appears that those regression
 333 maps are capturing features corresponding to κ and MEAN.

334 In order to quantify these visual observations, covariates are regressed on the reduced space. The root
 335 mean square error (RMSE) and the maximum error M are determined in a leave-one-out procedure. The
 336 results are given in Table 2. It can be noted that the MEAN strategy gives the same values for the graph
 337 metric degree D for all graphs since the number of edges is set to be the same for all graphs.



324 **Figure 3.** Standard ISOMAP reduced space representation of the original dataset. P_i : (comatose) patient $\#i$; C_j : control $\#j$. Covariates are mapped
 325 onto the reduced space (covariate value is color-coded). Top left: κ index mapping; top right: MEAN mapping; bottom left: LDA mapping; bottom right: FS
 326 mapping.

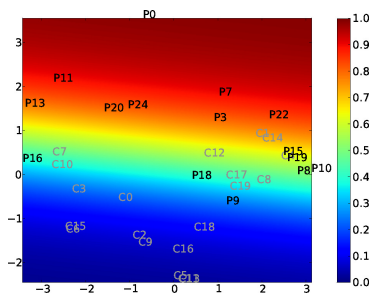
341 In this table, the lower the values, the better the adequacy with the reduced space. It appears that κ is the
 342 best choice across all metrics, except for *Eglob* where it is outperformed by MEAN. In the case of *Eglob*,
 343 this suggests that both κ and MEAN scores correspond to degrees of freedom of the intrinsic manifold of
 344 the functional connectivity graphs.

345 Figure 4 displays the probability of belonging to a specific class computed using logistic regression on
 346 the reduced space stemming from standard ISOMAP. The probability of belonging to the comatose class
 347 is color-coded in Figure 4.

349 This probability estimation using logistic regression is compared with covariates such as κ or MEAN, in
 350 Table 3. A high correlation score is observed between κ and logistic regression probability. The
 351 correlation score between the MEAN coefficient and the probabilistic mapping is lower than the one with
 352 κ as expected.

Covariate	<i>Eglob</i>	<i>Eglob</i>	<i>Clust</i>	<i>Clust</i>	<i>D</i>	<i>D</i>
	RMSE	M	RMSE	M	RMSE	M
κ	0.51	2.44	0.68	2.59	0.26	2.14
<i>LDA</i>	0.97	7.97	0.9	5.44	0.66	4.13
<i>FS</i>	0.64	2.2	1.1	9.12	0.83	7.49
<i>MEAN</i>	0.15	0.73	1.02	5.44		

338 **Table 2.** Assessment of the regression of covariates on the reduced space. Three different reduced spaces are at stake, one for each graph metric. Root mean
 339 square error (RMSE) and maximal error M are displayed. The MEAN strategy is not relevant for the degree D since the degrees D for all graphs are equal (the
 340 number of edges is set to be the same for all graphs).



348 **Figure 4.** Logistic regression using reduced space stemming from standard ISOMAP. The color codes the probability of belonging to the comatose class.

355 Taken together, these observations demonstrate the importance of κ in the classification of these
 356 populations. Obviously, for the special case of global efficiency metric, the MEAN score describes
 357 correctly the reduced space, but does not correspond to the classification pattern.

358 ***Covariate constrained manifold learning***

359 *Comatose population* First we evaluate the convergence of the optimization problem (Algorithm 1). To
 360 assess the difficulty of the optimization problem, we ran it with 500 random initializations. Only 63% of
 361 the runs converged to the same solution, whereas 37% of the runs converged to a local (worse) optimum.
 362 It thus appears that our initialization procedure addresses the local optimum issue. Nevertheless, this
 363 optimization problem would probably deserve further investigations which are out of the scope of this
 364 paper.

Coefficients	<i>Eglob</i>	<i>Clus</i>	<i>D</i>
κ	0.87	0.87	0.81
<i>MEAN</i>	0.55	0.42	

353 **Table 3.** Correlation scores between the probabilistic mapping and the different coefficients (κ index and MEAN measure). A high correlation score of the
 354 κ index indicates a good fitting between the reduced space representation and the classification of the two groups. The p -values are all smaller than 10^{-12} .

365 In Figure 5, we display the reduced space corresponding to our new manifold learning algorithm. We can
 366 observe that the two populations are well discriminated in the case of κ , but not for the MEAN
 367 coefficient. This is quantified by applying a classical SVM procedure in the reduced space. The obtained
 368 results are the following: for CCML 1; for ISOMAP 0.86; for LDA 0.91 ; for κ , 0.89 and for MEAN and
 369 FS 0.57.

370 We observe the strong interaction between κ and the MEAN in the top right of Figure 5, where the
 371 reduced space on one axis is κ and the mapping corresponds to the MEAN. To quantify this, in the case
 372 of κ , we estimate the correlation between the second coordinate and the MEAN score. The obtained
 373 score equals to 0.92, which confirms the intrinsic relationship between κ and the MEAN coefficient.

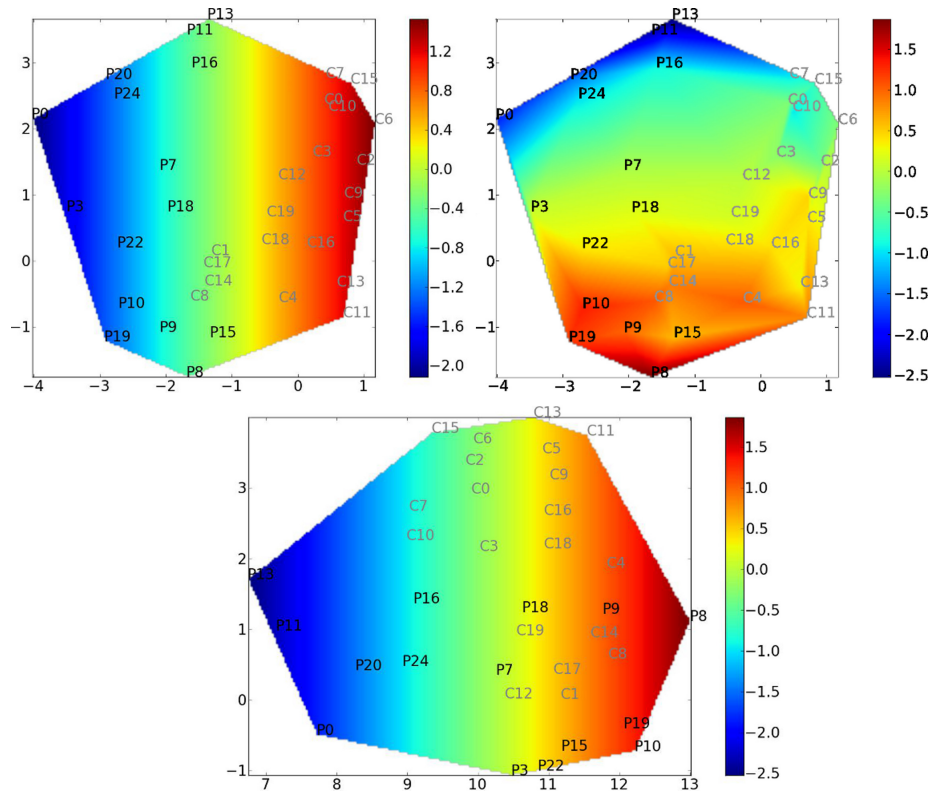
382 *Elderly and young population* The elderly and young groups are investigated in this section.

389 In Figure 6, the manifold obtained by standard ISOMAP is displayed. It is interesting to highlight that the
 390 κ index is not a pertinent feature to discriminate the old from the young, whereas the MEAN is a better
 391 discriminating feature. In both cases, the interpretation of the mapping is complex since it is not smooth.

392 In Figure 7, results from CCML are displayed for the MEAN coefficient. We can observe that the MEAN
 393 mapping discriminates the two groups.

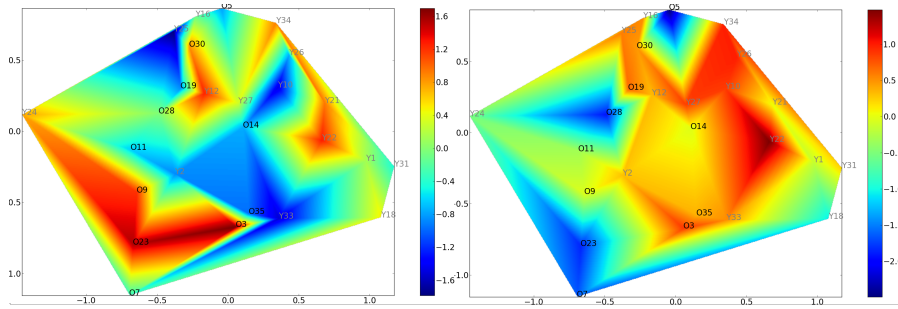
394 ***Application: a generative model for the prediction of the variation in a subject with regard to the changes of a***
 395 ***covariate***

396 Using the algorithm detailed in the last section, a map of the population is determined, with one of the
 397 reduced coordinates corresponding to a chosen covariate. To highlight the potential of the proposed

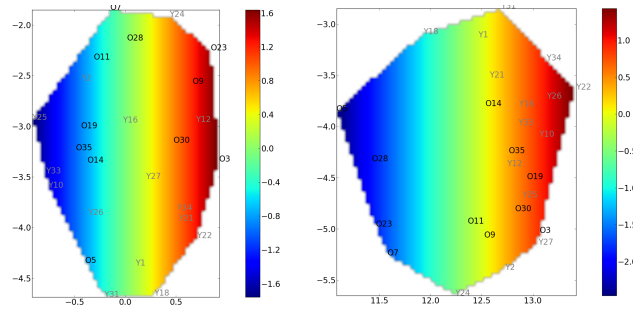


374 **Figure 5.** Covariate mapping onto the reduced space given by our method CCML using global efficiency as graph metric. The reduced space is computed
 375 using E_{glob} as a graph metric (the y_i 's). Covariate value is color-coded. For each subfigure, the coordinates correspond to $[\alpha c_i; x_i]^T$, where c_i is the
 376 constrained variable and x_i the free parameter. Top left: κ mapping with a κ -constrained reduced space, Top right: MEAN mapping with a κ -constrained
 377 reduced space; Bottom : MEAN mapping with a MEAN-constrained reduced space. As expected, we can observe that the mappings correlate well with the
 378 first coordinate by construction (top left and bottom). It is also clear that using a κ -constrained reduced space is facilitating the discrimination between the two
 379 populations. Indeed, the controls and patients are not covering the same part of the reduced space. On the contrary, as expected using the MEAN-constrained
 380 reduced space, the method is not providing a very clear discrimination between patients and controls. Especially, patients 9 and 18 are very close to controls.
 381 Finally, the top right figure is showing a correlation between the second coordinate of CCML and the MEAN.

398 method, we compute the transformation of a patient with regard to the changes of a covariate by creating
 399 a map from the reduced space back to the original space where we can make brain-related interpretations.
 400 This gives insight into the effect of the covariate on the patient. To perform this analysis, a regression is
 401 used to map the reduced space to the initial space (we used MARS regression (Friedman, 1991),
 402 coordinate-wise). This application is illustrated in Figure 8.



383 **Figure 6.** Left: κ mapping with the standard ISOMAP reduced space, Right: MEAN mapping with the same reduced space using global efficiency as graph
 384 metric. The old controls (resp. young controls) are labeled O (resp. Y). For these groups, the κ index cannot discriminate the two groups. However the MEAN
 385 index behaves better for the discrimination between the two groups. In each case, the interpretation is complex since the mapping of the covariate is not linear.

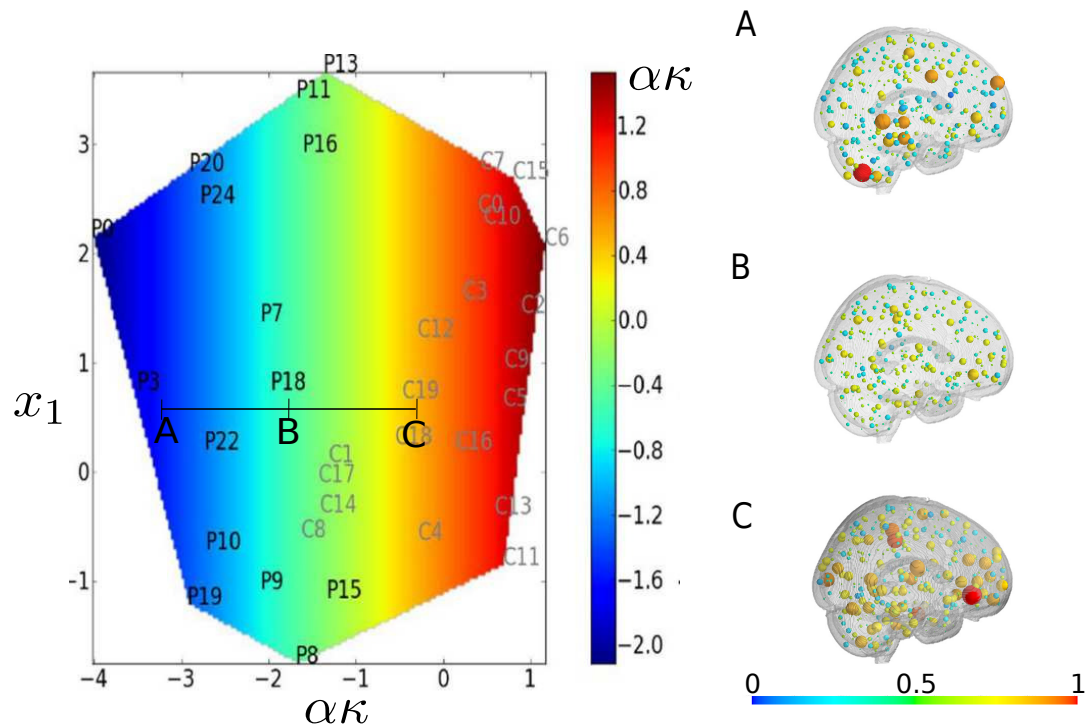


386 **Figure 7.** CCML approach using global efficiency as graph metric. Left: κ mapping with the κ -constrained reduced space, Right: MEAN mapping with
 387 the MEAN-constrained reduced space. The old controls (resp. young controls) are labeled O (resp. Y). Two manifolds (one for each constraint) have been
 388 determined. However only the MEAN-constrained manifold discriminates both groups.

DISCUSSION

408 *Assessment of graph metric descriptors*

409 The handcrafted design of graph metric descriptors is interesting since such descriptors carry
 410 straightforward physical meaning, like the κ index for hub reorganization. However, in a classification
 411 framework, such new scalar descriptors may not be optimal. To assess the pertinence of a new *ad hoc*
 412 graph metric descriptor for a classification task, it will be interesting to confront it to specific scalar
 413 coefficients used in standard classification algorithms (like LDA or FS), and examine if there is some
 414 correlation between the scalars at stake. It is also worth mentioning that other approaches are dedicated
 415 to classifications using directly the connectivity matrices (Dadi et al., 2019; Richiardi et al., 2013).
 416 Usually, the objective of these approaches is to obtain classification scores, i.e. assign a subject to a



403 **Figure 8.** Variation in one patient along the covariate axis using global efficiency as graph metric. The size and the color of the nodes on the right part of the
 404 figure are proportional to the graph metric, global efficiency, at each node. We consider the patient P18 in state B in the reduced space (left part of the figure).
 405 We predict its changes when the κ index is decreased (point A) or increased (point C). Intuitively, point A and point C correspond respectively to a degradation
 406 and to an improvement of the health of the patient. Interestingly, these trends can be directly observed in the graph space for clinical insights (right part of the
 407 figure). It can be noticed that the variations are not linear.

417 group, patient or control. To our knowledge, these approaches do not allow to explore the underlying
 418 brain mechanisms at the nodal level using the results of classification (Ktena et al., 2018; Kumar et al.,
 419 2018; Yamin et al., 2019). Graph metrics are known to capture important topological indicators in
 420 networks which are impossible to capture using classical data mining approaches (Zanin et al., 2016) or
 421 network embedding (Rosenthal et al., 2018).

422 *No free lunch for graph metric descriptors*

423 We hypothesize that there is no best descriptor adapted to all datasets. The optimality depends on 1) the
 424 kind of the data and 2) the kind of question/task addressed. This idea is known as the "no free lunch

425 theorem” (Wolpert, 1996): if an algorithm performs well on a certain class of problems then it has
426 necessarily poorer performances on the set of all remaining problems.

427 In the present study, we showed that the κ index yields good classification performances in separating a
428 comatose population from a healthy population. However the MEAN index better describes the groups of
429 elderly and young people (see Fig. 3): for this dataset, the κ index cannot separate the two groups, but the
430 MEAN score can. It is interesting to notice that several descriptors can map correctly a population, while
431 providing different information.

432 The ”no free lunch theorem” also applies to manifold learning algorithms. The underlying question is the
433 one of choosing an interpoint distance in the data space. A given interpoint distance will yield a specific
434 structure of samples in the reduced space. Therefore, the retained interpoint distance chosen will depend
435 on the final goal: mimicking the structure of the initial data points, enhancing class separation with a
436 view to achieving better classification performances, focusing on a specific property of the data,
437 etc... The proposed algorithm CCML aims at mimicking the structure of the initial data points, and this
438 to be done using explicitly a particular characteristic, chosen and imposed by the investigator.

439 *Manifold learning for brain graph analysis*

440 Manifold learning is well suited for brain graph analysis for several reasons. Firstly, global descriptors of
441 graph metrics represent an entire graph by a scalar value, which is generally ultimately insufficient to
442 model correctly the complexity of a graph population. Manifold learning is better suited to capturing the
443 complexity and variability of a given graph population, since more degrees of freedom are structuring the
444 reduced space.

445 Secondly, connectomes have been studied for their capacity to represent the brain as a system and not
446 merely as a juxtaposition of independent anatomical/functional regions. Classical statistical tests are not
447 adapted to analyze joint variations between local descriptors of graph metrics since those tests assume
448 independence between features. Brain graph manifold learning for comparing groups of graphs is
449 promising because joint variations are accounted for.

450 Thirdly, manifold learning may be turned to a generative model, when resorting to a mapping from the
451 reduced space to the data space. Brain graph manifold learning can be seen as a trade-off between global

452 and local brain graph metrics analysis. In other words, manifold learning is considered as a model at the
453 level of the group while preserving the information of the individuals. However this technique is hard to
454 interpret by its own. The addition of explicative covariables as proposed with the CCML method can
455 provide an understandable and generative model of population with the possibility of focusing at the
456 individual level (Costa et al., 2015). Using either global or local metrics is usually a hard task to
457 appropriately link these features to clinical information. Statistical approaches suffer from a lack of
458 interpretability where null and alternative hypothesis are tested. This is usually the case for coma studies
459 where simple univariate statistical tests are computed on graph metrics (Demertzi et al., 2014;
460 Malagurski et al., 2019). Using manifold learning, as illustrated in Fig. 8, it is possible to provide a
461 smooth description of the changes of the brain graphs of the patient in the reduced space. This approach
462 is very well adequate to relate the changes in brain connectivity along with the changes in clinical
463 features. More generally, manifold learning can be an interesting solution for personalized and predictive
464 medicine purposes. In our paper, we illustrate the result of our new proposed approach CCML on one
465 graph metric, namely global efficiency. However, including several graph metrics is also a possibility and
466 would lead to a more accurate description of the data, maybe at the cost of interpretability.

CONCLUSION

467
468 The originality and contribution of this paper is the devising of a nonlinear manifold model of brain
469 graph metrics. The essence of the approach is the capture of a metric through all nodes of a graph, across
470 all graphs of an entire population: a population of graphs is represented by a population of vectors, each
471 vector holding the variation of a metric through the nodes at stake. The population is then represented in
472 a reduced space. This is to be opposed to the standard representation of a given brain graph by a mere
473 scalar.

474 The proposed approach has several advantages. First and foremost, the data are represented with several
475 degrees of freedom, corresponding to the dimensions of the reduced space. The structure of the original
476 data set is captured by a compact representation. This allows to account for the complex variability of
477 populations of brain graphs. Secondly, such an approach naturally offers analysis of joint variations of

478 those brain graph metrics. Besides, the investigator has the possibility to analyze the data at the
479 population scale and simultaneously at the individual scale.

480 The investigation tool corresponding to the proposed approach allowed us to retrospectively assess the
481 hub disruption index (HDI), denoted κ , and proposed in one of our former works. Earlier work showed
482 that κ is a very good candidate for discriminating patients and controls in the case of coma.

483 Retrospectively, its performances are here assessed in comparison with machine learning methods
484 dedicated to linear group classification such as LDA. Besides yielding nice classification performances,
485 the present study showed that an advantage of κ , put in the perspective of a manifold model, is to give
486 clinical clues related to the pathology mechanism.

487 We observed strong relationships between scalar coefficients such as κ and MEAN, and the coordinates
488 of the manifold. It is important to notice that MEAN, which can separate groups in several pathologies
489 ([Lynall et al., 2010](#); [Supekar et al., 2008](#)), is not able to discriminate the comatose patients from the
490 normal population. However it brings additional information in terms of description of the population.
491 The manifold at stake shows that a scalar coefficient cannot capture the whole information encapsulated
492 in the graphs. One interest of manifold learning, and more specifically our new proposed method, is its
493 ability to reach a new level of interpretation of the brain graph metrics and the interaction between them.

ACKNOWLEDGMENTS

494 We want to thank the anonymous reviewers for their suggestions which improve significantly the quality
495 of our paper.

AUTHOR CONTRIBUTIONS

496 This project was formulated by FR, CH and SA based on substantial data, analyses and experiments of
497 FR, CH, MB, MS, FS, SK and SA. FR and SA formalised the model, implemented and ran the model;
498 FR, CH and SA wrote the manuscript.

REFERENCES

499 Achard, S., & Bullmore, E. (2007). Efficiency and cost of economical human brain functional networks. *PLoS Computational*

500 *Biology*, 3, e17.

501 Achard, S., Delon-Martin, C., Vértes, P. E., Renard, F., Schenck, M., Schneider, F., ... Bullmore, E. T. (2012, Nov.). Hubs of
502 brain functional networks are radically reorganized in comatose patients. *Proceedings of the National Academy of*
503 *Sciences*, 109(50), 20608-20613.

504 Aljabar, P., Wolz, R., & Rueckert, D. (2012). Manifold learning for medical image registration, segmentation and
505 classification. In K. Suzuki (Ed.), *Machine learning in computer-aided diagnosis: medical imaging intelligence and*
506 *analysis*. IGI Global.

507 Bellman, R. E. (1961). *Adaptive control processes - A guided tour*. Princeton University Press.

508 Brucher, M., Heinrich, C., Heitz, F., & Armspach, J. (2008). A metric multidimensional scaling-based nonlinear manifold
509 learning approach for unsupervised data reduction. *EURASIP J. Adv. Sig. Proc.*, 2008.

510 Bullmore, E., & Sporns, O. (2009a, feb). Complex brain networks: graph theoretical analysis of structural and functional
511 systems. *Nature Reviews Neuroscience*, 10(3), 186–198.

512 Bullmore, E., & Sporns, O. (2009b, Mar). Complex brain networks: graph theoretical analysis of structural and functional
513 systems. *Nat Rev Neurosci*, 10(3), 186–198. Retrieved from <http://dx.doi.org/10.1038/nrn2575> doi:
514 10.1038/nrn2575

515 Costa, L., Smith, J., Nichols, T., Cussens, J., Duff, E. P., Makin, T. R., et al. (2015). Searching multiregression dynamic
516 models of resting-state fmri networks using integer programming. *Bayesian Analysis*, 10(2), 441–478.

517 Dadi, K., Rahim, M., Abraham, A., Chyzyk, D., Milham, M., Thirion, B., ... others (2019). Benchmarking functional
518 connectome-based predictive models for resting-state fmri. *Neuroimage*, 192, 115–134.

519 Demertzi, A., Gomez, F., Crone, J. S., Vanhaudenhuyse, A., Tshibanda, L., Noirhomme, Q., ... others (2014). Multiple fmri
520 system-level baseline connectivity is disrupted in patients with consciousness alterations. *Cortex*, 52, 35–46.

521 Fallani, F. D. V., Richiardi, J., Chavez, M., & Achard, S. (2014). Graph analysis of functional brain networks: practical issues
522 in translational neuroscience. *Philosophical Transactions of the Royal Society B: Biological Sciences*, 369(1653),
523 20130521. Retrieved from
524 <http://rstb.royalsocietypublishing.org/content/369/1653/20130521.short> doi:
525 10.1098/rstb.2013.0521

526 Filippi, M., Valsasina, P., Sala, S., Martinelli, V., Ghezzi, A., Veggiotti, P., ... Rocca, M. (2014). Abnormalities of the brain
527 functional connectome in pediatric patients with multiple sclerosis. *Neurology*, 82(10 Supplement).

528 Fisher, R. A. (1936). The use of multiple measurements in taxonomic problems. *Annals of Eugenics*, 7(2), 179–188. doi:
529 10.1111/j.1469-1809.1936.tb02137.x

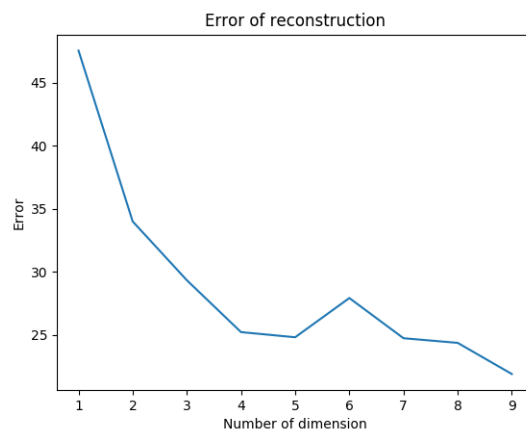
- 530 Friedman, J. (1991, March). Multivariate adaptive regression splines. *Annals of Statistics*, 19(1), 1–67.
- 531 Gallos, I., & Siettos, C. (2017). Classification of fmri resting-state maps using machine learning techniques: A comparative
532 study. In *Aip conference proceedings* (Vol. 1906, p. 200001).
- 533 Gerber, S., Tasdizen, T., Thomas Fletcher, P., Joshi, S., & Whitaker, R. (2010, Oct.). Manifold modeling for brain population
534 analysis. *Medical Image Analysis*, 14(5), 643–653.
- 535 Haak, K. V., Marquand, A. F., & Beckmann, C. F. (2018). Connectopic mapping with resting-state fmri. *Neuroimage*, 170,
536 83–94.
- 537 Hastie, T., Tibshirani, R., & Friedman, J. (2001). *The elements of statistical learning*. Springer.
- 538 Hearst, M. A., Dumais, S. T., Osuna, E., Platt, J., & Scholkopf, B. (1998). Support vector machines. *IEEE Intelligent Systems
539 and their applications*, 13(4), 18–28.
- 540 Huo, X., Ni, X. S., & Smith, A. K. (2007). A survey of manifold-based learning methods. *Recent advances in data mining of
541 enterprise data*, 691-745.
- 542 Ktena, S. I., Parisot, S., Ferrante, E., Rajchl, M., Lee, M., Glocker, B., & Rueckert, D. (2018). Metric learning with spectral
543 graph convolutions on brain connectivity networks. *NeuroImage*, 169, 431–442.
- 544 Kumar, K., Toews, M., Chauvin, L., Colliot, O., & Desrosiers, C. (2018). Multi-modal brain fingerprinting: a manifold
545 approximation based framework. *NeuroImage*, 183, 212–226.
- 546 Latora, V., & Marchiori, M. (2001, Oct). Efficient behavior of small-world networks. *Physical Review Letters*, 87, 198701.
- 547 Laurienti, P. J., Bahrami, M., Lyday, R. G., Casanova, R., Burdette, J. H., & Simpson, S. L. (2019). Using low-dimensional
548 manifolds to map relationships between dynamic brain networks. *Frontiers in human neuroscience*, 13, 430.
- 549 Lawrence, N. D. (2004). Gaussian process latent variable models for visualisation of high dimensional data. In *Advances in
550 neural information processing systems* (Vol. 16, pp. 329–336).
- 551 Lynall, M.-E., Bassett, D. S., Kerwin, R., McKenna, P. J., Kitzbichler, M., Muller, U., & Bullmore, E. (2010). Functional
552 connectivity and brain networks in schizophrenia. *The Journal of Neuroscience*, 30(28), 9477-9487.
- 553 Malagurski, B., Péran, P., Sarton, B., Vinour, H., Naboulsi, E., Riu, B., . . . others (2019). Topological disintegration of resting
554 state functional connectomes in coma. *NeuroImage*, 195, 354–361.
- 555 Meunier, D., Achard, S., Morcom, A., & Bullmore, E. (2009). Age-related changes in modular organization of human brain
556 functional networks. *Neuroimage*, 44(3), 715–723.
- 557 Mheich, A., Hassan, M., Khalil, M., Gripon, V., Dufor, O., & Wendling, F. (2017). Siminet: a novel method for quantifying
558 brain network similarity. *IEEE transactions on pattern analysis and machine intelligence*, 40(9), 2238–2249.
- 559 Mokhtari, F., & Hossein-Zadeh, G.-A. (2013, 1). Decoding brain states using backward edge elimination and graph kernels in

- 560 fMRI connectivity networks. *Journal of neuroscience methods*, 212(2), 259-268.
- 561 Mwangi, B., Tian, T. S., & Soares, J. C. (2014). A review of feature reduction techniques in neuroimaging. *Neuroinformatics*,
562 12(2), 229–244.
- 563 Newman, M. E. J. (2002, Oct). Assortative mixing in networks. *Physical Review Letters*, 89, 208701.
- 564 Newman, M. E. J. (2006). Modularity and community structure in networks. *Proceedings of the National Academy of*
565 *Sciences*, 103(23), 8577-8582.
- 566 Pedregosa, F., Varoquaux, G., Gramfort, A., Michel, V., Thirion, B., Grisel, O., . . . Duchesnay, E. (2011). Scikit-learn:
567 Machine learning in Python. *Journal of Machine Learning Research*, 12, 2825–2830.
- 568 Renard, F., Heinrich, C., Achard, S., Hirsch, E., & Kremer, S. (2012). Statistical kernel-based modeling of connectomes. In
569 *Proc. int workshop on pattern recognition in NeuroImaging* (p. 69-72).
- 570 Richiardi, J., Achard, S., Bullmore, E., & Vile, D. V. D. (2011). Classifying connectivity graphs using graph and vertex
571 attributes. In *Proc. int workshop on pattern recognition in NeuroImaging*. Seoul, Korea.
- 572 Richiardi, J., Achard, S., Bunke, H., & Van De Ville, D. (2013). Machine learning with brain graphs: predictive modeling
573 approaches for functional imaging in systems neuroscience. *IEEE Signal Processing Magazine*, 30(3), 58–70.
- 574 Robinson, E. C., Hammers, A., Ericsson, A., Edwards, A. D., & Rueckert, D. (2010, April). Identifying population
575 differences in whole-brain structural networks: a machine learning approach. *NeuroImage*, 50(3), 910–919.
- 576 Rosazza, C., & Minati, L. (2011). Resting-state brain networks: literature review and clinical applications. *Neurological*
577 *sciences*, 32(5), 773–785.
- 578 Rosenthal, G., Váša, F., Griffa, A., Hagmann, P., Amico, E., Goñi, J., . . . Sporns, O. (2018). Mapping higher-order relations
579 between brain structure and function with embedded vector representations of connectomes. *Nature communications*,
580 9(1), 1–12.
- 581 Saggari, M., Sporns, O., Gonzalez-Castillo, J., Bandettini, P. A., Carlsson, G., Glover, G., & Reiss, A. L. (2018). Towards a
582 new approach to reveal dynamical organization of the brain using topological data analysis. *Nature communications*,
583 9(1), 1–14.
- 584 Sfikas, G., & Nikou, C. (2016). Bayesian multiview manifold learning applied to hippocampus shape and clinical score data.
585 In *Medical computer vision and Bayesian and graphical models for biomedical imaging – MICCAI 2016* (pp.
586 160–171). Springer.
- 587 Sporns, O., Tononi, G., & Kötter, R. (2005). The human connectome: a structural description of the human brain. *PLoS*
588 *Computational Biology*, 1(4), e42.
- 589 Supekar, K., Menon, V., Rubin, D., Musen, M., & Greicius, M. D. (2008, June). Network analysis of intrinsic functional brain

- 590 connectivity in alzheimer’s disease. *PLoS Computational Biology*, 1–11.
- 591 Tenenbaum, J. B., de Silva, V., & Langford, J. C. (2000, December). A global geometric framework for nonlinear
592 dimensionality reduction. *Science*, 290(5500), 2319–2323.
- 593 Tzourio-Mazoyer, N., Landeau, B., Papathanassiou, D., Crivello, F., Etard, O., Delcroix, N., . . . Joliot, M. (2002). Automated
594 anatomical labeling of activations in spm using a macroscopic anatomical parcellation of the mni mri single-subject
595 brain. *Neuroimage*, 15(1), 273–289.
- 596 Watts, D. J., & Strogatz, S. H. (1998). Collective dynamics of ‘small-world’ networks. *nature*, 393(6684), 440.
- 597 Webb, A. (2002). *Statistical pattern recognition* (second ed.). Wiley.
- 598 Wolpert, D. H. (1996). The lack of a priori distinctions between learning algorithms. *Neural computation*, 8(7), 1341–1390.
- 599 Yamin, A., Dayan, M., Squarcina, L., Brambilla, P., Murino, V., Diwadkar, V., & Sona, D. (2019). Comparison of brain
600 connectomes using geodesic distance on manifold: A twins study. In *2019 IEEE 16th International Symposium on*
601 *Biomedical Imaging (ISBI 2019)* (pp. 1797–1800).
- 602 Zanin, M., Papo, D., Sousa, P. A., Menasalvas, E., Nicchi, A., Kubik, E., & Boccaletti, S. (2016). Combining complex
603 networks and data mining: why and how. *Physics Reports*, 635, 1–44.

A: ELBOW CURVE

The choice for the dimension 2 of the reduced space takes into account mainly the ability to interpret the results. However, we checked also the curve of the error of the fitting, *refelbow*. This shows clearly that the dimension 2 is a good trade-off between minimisation of error and visualisation, it may be also worth exploring the dimension 3.



604

Figure A.1. Elbow curve